Crossed diagrams for transport in substitutional binary alloys

S. M. Chitanvis
Department of Physics, City College of the City University of New York, New York, New York 10031
(Received 1 August 1984)

We have adapted the method of summing crossed diagrams to the case of substitutional binary alloys. The summation is done by explicitly uncrossing the diagrams to look like ladders. Details are presented for the case of a single-band model of a simple-cubic lattice with nearest-neighbor hopping. The critical concentration at which the conductivity goes to zero is estimated. Some aspects of the generalization of this method to realistic models of binary alloys are discussed.

I. INTRODUCTION

In a formulation of the average conductivity of a realistic multiorbital model of a substitutional binary-alloy semiconductor (Hg_{1-x} Cd_x Te) within the coherent potential approximation (CPA), it was discovered that[1] (1) the vertex corrections do not vanish due to a mixing of the various (s, p,...) orbitals, and (2) the conductivity is divergent unless the infinite-volume limit is taken before the zero-frequency limit is reached.

The physical interpretation is that when considering the static conductivity of a finite sample, one must be careful to attach the sample to external leads, which in turn are attached to a dc voltage source.[2] This is because the concept of the conductivity of an isolated, finite sample is not very meaningful. For an infinite sample, however, such considerations are not important. Chitanvis and Raghavan[1] conjectured that the divergence was not simply a quirk of the CPA, but rather, a more general malaise due the quenched nature of the disorder. They also conjectured that when the lattice was allowed to vibrate, bremsstrahlung would take care of the infrared divergence as it does in quantum electrodynamics.[3]

In order to test the first conjecture, we looked at the hierarchy of traveling cluster approximations (TCA),[4,5] which is a generalization of the CPA, for a single-band model (generalization to more complicated models is not expected to change our conclusion). Higher-order diagrams occurring in the TCA ensure that the conductivity vertex corrections do not vanish.[6] In fact they diverge if the limiting processes mentioned above are handled in a cavalier fashion. On the other hand, if the static limit is taken carefully, one finds compensating diagrams[1,6] that exactly cancel each other. In other words, the proper limiting procedure gives no vertex corrections at all. This surprising cancellation occurs in all finite orders of the TCA hierarchy (we note that such cancellations have no chance of occurring in calculations of $\langle\ |\ G_{00}\ |^2\ \rangle$).[5] Therefore, within the TCA, one can never obtain higher-order corrections to the conductivity. The proof may be obtained by combining the single-band formalism of Chitanvis and Leath[5] with the analysis of Chitanvis and Raghavan,[1] and may be presented in a future publication. One may now wonder where the higher-order (vertex) corrections to the static conductivity will come from.

In an effort to locate nonvanishing vertex corrections, we now describe a modest effort in which we have adapted to the case of substitutional binary alloys the method of summing maximally crossed diagrams,[7,8] which has been argued to give the dominant contribution to the conductivity in the metallic regime.[8] This way, one would have a good measure of the resistance of alloys in the regime of extended states. While work on this problem was in progress, we discovered an effort similar to ours had been reported by Bhatt and Ramakrishnan.[9] The formalism of Bhatt and Ramakrishnan[9] applies to an amorphous system without short-range order. They have shown that electron-electron interactions are not necessarily important. We have therefore ignored them in our report here. In the future we plan to extend our method to realistic models of alloys.

II. CROSSED DIAGRAMS

Abrahams and Ramakrishnan[10] considered the set of diagrams for static conductivity, which are obtained by crossing ladders of all orders. The diagrams we consider are those obtained by "crossing" diagrams of all orders in the CPA formulation of the vertex correction.[1,11] The CPA diagrams are of course "ladders". One immediately notices that higher-order crossed diagrams may be obtained by crossing the diagrams obtained within each level of the TCA hierarchy[4,5]—the TCA being a natural generalization of the CPA. We thus conceive our own hierarchy of approximations, based on crossing those diagrams that appear in the TCA hierarchy. We must point out that our new set of approximations, though comprised of diagrams beyond those of Abrahams and Ramakrishnan,[10] does not hold out the promise of being able to give more information of "localization" per se. This is because we do not expect the infrared divergence in one and two dimensions to worsen in our hierarchy.[5,8]

Our general formalism applies to any Hamiltonian describing diagonal disorder [see, e.g., Eq. (2.4)]:

$$H = H_0 + \sum_i V_i,$$

with

$$p(V_i) = c_A\ \delta(V_i - V_A) + (1 - c_A)\ \delta(V_i - V_B),$$

where $p(V_i)$ is the distribution function for V_i.

We obtain more specific results for a single-band model of a simple cubic lattice in three dimensions with nearest-neighbor hopping:

$$H = t \sum_i |i_{\mathrm{NN}}\rangle \Big\langle i\Big| + \mathrm{H.c.} + \sum_i \Big|i\Big\rangle \epsilon_i \langle i|,$$

where the subscript NN stands for nearest-neighbors, and where ϵ_i is a scalar site energy given by the binary distribution

$$p(\epsilon_i) = c_A\, \delta(\epsilon_i - \epsilon_A) + (1 - c_A)\, \delta(\epsilon_i - \epsilon_B).$$

The hopping term in the above equation represents the unperturbed Hamiltonian H_0.

The details of the augmented space formalism (ASF), according to which diagrams are drawn, have been delineated explicitly by Chitanvis and Leath[5] and Chitanvis and Raghavan.[1] It is well known[1] that to compute the conductivity $\sigma = \langle \hat{v} G^\dagger \hat{v} G^\dagger \rangle$ we need an operator of the form $K = G^\dagger (\hat{v} + \Gamma) G$, where $\hat{v}$ is the velocity operator and Γ is the vertex function. In k space $\mathbf{v}(k) = \nabla_k H_0(\mathbf{k})$. Given these rules, the first-order crossed diagram is drawn in Fig. 1 and the corresponding analytic expression is

$$\Gamma_x^{(1)} = V_{j_0}^- \mathcal{G}^{\dagger\{j_0\}} V_j^- (\mathcal{G}^{\dagger\{j\}} \hat{v} \mathcal{G}^{\{j_0\}}) V_{j_0}^- \mathcal{G}^{\{j\}} V_j^-. \tag{2.1}$$

Let us define $\hat{Q}$ by $\mathcal{G}^{\dagger\{j\}} \hat{v} \mathcal{G}^{\{j_0\}}$. We now consider the coefficient of $\hat{Q}$ in Eq. (2.1). The purpose is to be able to write the resultant expression in such a manner that it appears "uncrossed". We therefore use the resolution of the identity $\mathbb{1} = \sum_i |i\rangle\langle i|$, where i corresponds to a site. This is inserted to the right and left of the parentheses in Eq. (2.1) so that the truncated operator (coefficient of $\hat{Q}$) mentioned above may be defined as

$$\Gamma_x^{(1)j}(j_0) = \langle j_0 | V_{j_0}^- \mathcal{G}^{\dagger\{j_0\}} V_j^- | j \rangle \langle j_0 | V_{j_0}^- \mathcal{G}^{\{j\}} V_j^- | j \rangle \tag{2.2a}$$

$$= [\langle j | V_j^- \mathcal{G}^{\{j_0\}} V_{j_0}^- | j_0 \rangle]^* \langle j_0 | V_{j_0}^- \mathcal{G}^{\{j\}} V_j^- | j \rangle. \tag{2.2b}$$

The asterisk in Eq. (2.2b) signifies a complex conjugate. Equation (2.2b) represents an "uncrossing" of Fig. 1, and is depicted in Fig. 2. The next maximally crossed diagram may be drawn in its "ladder" form and expressed as

$$\tilde{\Gamma}_x^{(2),j}(j_0) = \sum_{j''} [\langle j | V_j^- \mathcal{G}^{\{j''\}} V_{j''}^- \mathcal{G}^{\{j_0\}} V_{j_0}^- | j_0 \rangle]^* \langle j_0 | V_{j_0}^- \mathcal{G}^{\{j''\}} V_{j''}^- \mathcal{G}^{\{j\}} V_j^- | j \rangle. \tag{2.3}$$

Similar expressions may be written for higher-order diagrams. Their sum may be conveniently expressed in the form of an integral equation:

$$\Gamma_x^j(j_0) = [\cdot V_j^- \mathcal{G}^{\{j_0\}} V_{j_0}^- | j_0 \rangle]^* \langle j_0 | V_{j_0}^- \mathcal{G}^{\{j\}} V_j^- + \sum_{j' \neq j} [\cdot V_j^- \mathcal{G}^{\{j'\}}]^* \Gamma_x^{j'}(j_0) \mathcal{G}^{\{j\}} V_j^-. \tag{2.4}$$

This equation is in operator form. The dots under the complex-conjugation operation indicate that the conjugation operation is to be performed *after* the scalar product with a Dirac *bra* has been taken.

The corrections to the ladders are of order $||G_0 V_j^-||$. Thus summing crossed diagrams gives a good measure of the conductivity when this operator norm is small.

Equation (2.4) may be written in a matrix form for a single-band model. We emphasize that in Eqs. (2.1)—(2.4) and beyond, $j \neq j_0$:

$$\langle j | \Gamma_x^j(j_0) | j \rangle \equiv \Gamma_{xjj}(j_0)$$

$$= (\epsilon^-)^4 [\langle j | \mathcal{G}^{\{j_0\}} | j_0 \rangle]^* \langle j_0 | \mathcal{G}^{\{j\}} | j \rangle + (\epsilon^-)^2 \sum_{j' \neq j} [\langle j | \mathcal{G}^{\{j'\}} | j' \rangle]^* \langle j' | \mathcal{G}^{\{j\}} | j \rangle \Gamma_{xj'j'}(j_0). \tag{2.5}$$

Thus,

$$\Gamma_{xjj}(j_0) = f_j(j_0) + \sum_{j' \neq j} \underline{L}_{jj'} \Gamma_{xj'j'}(j_0), \tag{2.6a}$$

where

$$f_j(j_0) = (\epsilon^-)^4 [\langle j | \mathcal{G}^{\{j_0\}} | j_0 \rangle]^* \langle j_0 | \mathcal{G}^{\{j\}} | j \rangle \tag{2.6b}$$

and

$$\underline{L}_{jj'} = (\epsilon^-)^2 \sum_{j' \neq j} [\langle j | \mathcal{G}^{\{j'\}} | j' \rangle]^* \langle j' | \mathcal{G}^{\{j\}} | j \rangle. \tag{2.6c}$$

We now define the following Fourier transforms:

$$\hat{\underline{L}}_{\mathbf{p},\mathbf{p}'} = \sum_{jj'} \underline{L}_{jj'} (1 - \delta_{jj'}) e^{i(\mathbf{R}_j \cdot \mathbf{p} - \mathbf{R}_{j'} \cdot \mathbf{p}')}, \tag{2.7a}$$

$$\hat{f}_{\mathbf{p}}(j_0) = \sum_j f_j(j_0) e^{i\mathbf{R}_j \cdot \mathbf{p}}, \tag{2.7b}$$

$$\hat{\Gamma}_{x\mathbf{p}}(j_0) = \sum_j \Gamma_{xjj}(j_0) e^{i\mathbf{R}_j \cdot \mathbf{p}}. \tag{2.7c}$$

Equation (2.7a) reduces to

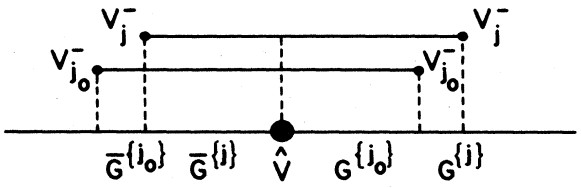

FIG. 1. The first-order crossed diagram corresponds to Eq. (2.1). The dotted lines have been added for easy readability.

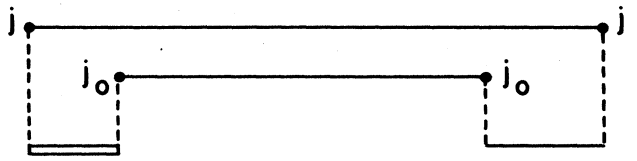

FIG. 2. This diagram corresponds to Eq. (2.2b), depicts the "uncrossing" of Fig. 1. The double baseline on the left-hand side indicates a complex-conjugate operation.

$$\hat{L}_{\mathbf{p},\mathbf{p}'} = \Omega_B\,\delta(\mathbf{p}-\mathbf{p}')\,|\gamma(z)|^2 \times\left[\int\frac{d^3s}{\Omega_B}\hat{G}(s)\hat{G}^*(|\mathbf{s}-\mathbf{p}|)\Theta(\mathbf{s}-\mathbf{p})-|G(0)|^2\right] \tag{2.8a}$$

$$\equiv \Omega_B\,\delta(\mathbf{p}-\mathbf{p}')l(\mathbf{p}), \tag{2.8b}$$

where

$$\gamma(z) = \frac{\epsilon^-}{1+G(0)(\omega-\epsilon^+)}, \tag{2.9}$$

and where $\hat{G}(p)$ is the Fourier transform of $G(|\mathbf{x}-\mathbf{x}'|)$ and $\Theta(\mathbf{s}-\mathbf{p})=1$ if $\mathbf{s}-\mathbf{p}$ lies in the first Brillouin zone, and zero otherwise. Equation (2.7b) may be written in the following form:

$$\hat{f}_{\mathbf{p}}(j_0) = |\epsilon^-\gamma(z)|^2\sum_{j\neq j_0}e^{i\mathbf{R}_{j_0}\cdot\mathbf{p}}|G(\mathbf{R}_{j_0}-\mathbf{R}_j)|^2 = (\epsilon^-)^2\,e^{(i\mathbf{R}_{j_0}\cdot\mathbf{p})}\,l(\mathbf{p}). \tag{2.10}$$

Given Eqs. (2.8a) and (2.8b), we see that the integral equation for $\hat{\Gamma}_{x\mathbf{p}}(j_0)$, obtained from Eq. (2.6) by utilizing Eqs. (2.7)—(2.8), becomes an algebraic one. Thus,

$$\hat{\Gamma}_{x\mathbf{p}}(j_0) = \frac{\hat{f}_{\mathbf{p}}(j_0)}{1-l(\mathbf{p})} \tag{2.11}$$

and

$$\hat{\Gamma}_{xjj}(j_0) = \int\frac{d^3p}{\Omega_B}\,\frac{\hat{f}_{\mathbf{p}}(j_0)}{1-l(\mathbf{p})}\,e^{-i\mathbf{p}\cdot\mathbf{R}_j}. \tag{2.12}$$

Now, the vertex function $\Gamma = \sum_j\Gamma_j$ is obtained by *undoing* the transformation that led us from Eq. (2.1) to (2.2b):

$$\Gamma_j = \sum_{j_0\neq j}\langle j|\mathcal{G}^{\dagger\{j\}}\hat{v}\,\mathcal{G}^{\{j_0\}}|j_0\rangle\,\Gamma_{xjj}(j_0) \tag{2.13}$$

whence $K = G^\dagger[\hat{v}+\Gamma]\,G$ may be computed:

$$\langle\mathbf{p}|\Gamma|\mathbf{p}\rangle = \frac{|\gamma(z)|^2}{(\epsilon^-)^2}\int\frac{d^3k}{\Omega_B}\,\hat{v}(\mathbf{k})\sum_{j,j_0}(1-\delta_{jj_0})\Gamma_{xjj}(j_0)e^{i\mathbf{R}_j\cdot(\mathbf{p}+\mathbf{k})}e^{-i\mathbf{R}_{j_0}\cdot(\mathbf{p}+\mathbf{k})} \tag{2.14}$$

$$= \int\frac{d^3k}{\Omega_B}\,|\gamma(z)|^2\,|\hat{G}(k)|^2\,v(\mathbf{k})\left[\frac{l(\mathbf{p}+\mathbf{k})}{1-l(\mathbf{p}+\mathbf{k})}-\frac{l(\mathbf{q})}{1-l(\mathbf{q})}\right]. \tag{2.15}$$

The first term in Eq. (2.15) above is recognized as the integral found by Abrahams *et al.*[8] to contribute to backscattering.

We eliminate the second term, using $\hat{v}(\mathbf{k})=-\hat{v}(-\mathbf{k})$ and $\hat{G}(-\mathbf{k})=\hat{G}(\mathbf{k})$, just as it was done by Velický.[11] We point out that had we used a realistic model of our binary alloy, such as the multiorbital model of Chen and Sher,[12] then the second term would not have vanished, as described by Chitanvis and Raghavan.[1] In fact, it would have diverged. This divergence can be eliminated by a proper limiting procedure, whose physical significance has been stressed in the Introduction.

From Chitanvis and Raghavan[1] the static conductivity $\sigma(\omega=0,T)=\kappa\tilde{\sigma}(\omega=0,T)$, $\kappa=e^2\hbar^2/4\pi$ is seen to be composed of two parts:

$$\tilde{\sigma}(\omega=0,T) = \tilde{\sigma}_0(\omega=0,T)+\delta\tilde{\sigma}(\omega=0,T), \tag{2.16}$$

$$\tilde{\sigma}_0(\omega=0,T) = 2\mathrm{Re}\int d\lambda\left[-\frac{\partial f(\lambda)}{\partial\lambda}\right]\int\frac{d^3k}{\Omega_B}\,|\mathbf{v}(k)|^2\hat{G}^\dagger(\lambda,k)G(\lambda,k), \tag{2.17}$$

$$\delta\tilde{\sigma}(\omega=0,T) = 2\mathrm{Re}\int d\lambda\left[-\frac{\partial f(\lambda)}{\partial\lambda}\right]\int\frac{d^3k}{\Omega_B}\int\frac{d^3p}{\Omega_B}\mathbf{v}(k)\cdot\mathbf{v}(p)\,|\gamma(\lambda)|^2\frac{|\hat{G}(\lambda,k)|^2|\hat{G}(\lambda,p)|^2}{1-l(\mathbf{p}+\mathbf{k})}. \tag{2.18}$$

Equation (2.17) corresponds to the nonvertex contribution to the conductivity, viz., the Ziman-Drude formula. The nonvanishing vertex correction given by Eq. (2.18) may be investigated by changing to "center-of-mass" and "relative" coordinates, viz., $\mathbf{K}=(\mathbf{k}'+\mathbf{p})/2$, $\mathbf{k}'=\mathbf{k}-\mathbf{p}$, and expanding $l(2\mathbf{K})=l(0)+4\mathbf{K}^2F(\lambda)$ [$l(0)=1$ by the Ward-Velický identity[1]] so that[8]

$$\delta\tilde{\sigma}(\omega=0,T)\approx\tfrac{1}{2}\,\mathrm{Re}\int d\lambda\left[-\frac{\partial f}{\partial\lambda}\right]\frac{|\gamma(\lambda)|^2}{F(\lambda)}\int\frac{d^3\mathbf{k}}{\Omega_B}\,|\hat{G}(\lambda,k)|^4\,|\mathbf{v}(k)|^2\int_0^{(1/l_{\mathrm{mfp}})}\frac{d^3K}{\Omega_B K^2} \tag{2.19}$$

$$=\int d\lambda\left[-\frac{\partial f}{\partial\lambda}\right]|\gamma(\lambda)|^2 2\mathrm{Re}\left[\frac{1}{F(\lambda)}\right]g(\lambda)\left[\frac{1}{\Omega_B\, l_{\mathrm{mfp}}}\right], \tag{2.20}$$

where l_{mfp} is the mean free path,

$$g(\lambda)=\int\frac{d^3k}{\Omega_B}\,|\hat{G}(\lambda,k)|^4\,|\nabla_{\mathbf{k}}H_0(\mathbf{k})|^2, \tag{2.21}$$

and

$$F(\lambda)=|\gamma(\lambda)|^2\int\frac{d^3k}{\Omega_B}G(\lambda,k)[G^*(\lambda,k)]^3\,|\nabla_{\mathbf{k}}H_0(\mathbf{k})|^2 \tag{2.22}$$

$$=|\gamma(\lambda)|^2\int\frac{d^3k}{\Omega_B}\int d\nu\;\delta(\nu-H_0(\mathbf{k}))\frac{1}{(\lambda-\nu-\Sigma)}\;\frac{1}{(\lambda-\nu-\Sigma)^{*3}}\,|\nabla_{\mathbf{k}}H_0(\mathbf{k})|^2 \tag{2.23}$$

$$\equiv|\gamma(\lambda)|^2\int d\nu\frac{\tilde{\rho}(\nu)}{(\lambda-\nu-\Sigma)(\lambda-\nu-\Sigma)^{*3}}, \tag{2.24}$$

where Σ is the self-energy due to averaging, and

$$\tilde{\rho}(\nu)=\int\frac{d^3k}{\Omega_B}\,\delta(\lambda-H_0(\mathbf{k}))\,|\nabla_{\mathbf{k}}H_0(\mathbf{k})|^2. \tag{2.25}$$

Since for small disorder $\mathrm{Re}\Sigma\approx|\,\mathrm{Im}\Sigma\,|\to 0^{\dagger}$ the most divergent part of $F(\lambda)$ is

$$F(\lambda)\approx-\frac{\tilde{\rho}(\lambda)}{[\mathrm{Im}\;\Sigma(\lambda)]^3}\,|\gamma(\lambda)|^2. \tag{2.26}$$

Similarly,

$$g(\lambda)\approx\frac{\tilde{\rho}(\lambda)}{[\mathrm{Im}\;\Sigma(\lambda)]^3}. \tag{2.27}$$

Hence we get

$$\delta\tilde{\sigma}(\omega=0,T)\approx(-1)\int d\lambda\left[-\frac{\partial f}{\partial\lambda}\right]\left[\frac{1}{\Omega_B l_{\mathrm{mfp}}(\lambda)}\right]. \tag{2.28}$$

The negative sign of this term is the signature of the crossed diagram—recall that $-\partial f/\partial\lambda\to\delta(\lambda-\mu)$, as $T\to 0$. We follow Abrahams *et al.* in taking $l_{\mathrm{mfp}}(\lambda)=v_F\tau$, $\tau^{-1}=|\,\mathrm{Im}\Sigma(\lambda)\,|/\hbar$. It is important to note that the approximations we used are valid in the middle of the band.

Equation (2.17) may also be similarly simplified in the limit of small disorder:

$$\tilde{\sigma}_0(\omega=0,T)$$

$$\approx\int d\lambda\left[-\frac{\partial f}{\partial\lambda}\right]\int\frac{d^3k}{\Omega_B}\,|\mathbf{v}(k)|^2\,|\,\mathrm{Im}G(\lambda,k)\,|^2 \tag{2.29}$$

$$\approx\int d\lambda\left[-\frac{\partial f}{\partial\lambda}\right]\left[\frac{\tilde{\rho}(\lambda)}{|\;\mathrm{Im}\;\Sigma(\lambda)\;|}\right]. \tag{2.30}$$

Therefore, at $T=0$

$$\tilde{\sigma}(\omega=0,T=0)\approx\left[\frac{\tilde{\rho}(\mu)}{|\;\mathrm{Im}\Sigma(\mu)\;|}-\frac{1}{\Omega_B l_{\mathrm{mfp}}(\mu)}\right]. \tag{2.31}$$

Since $|\,\mathrm{Im}\Sigma(\lambda)\,|\approx c(1-c)\,(\Delta\epsilon)^2\,\pi\rho_0(\lambda)$, where $\Delta\epsilon=\epsilon_A-\epsilon_B$, and $\rho_0(\lambda)$ is the density of states of the pure crystal, we obtain

$$\tilde{\sigma}(\omega=0,0)=\frac{\tilde{\rho}(\mu)}{c(1-c)\,(\Delta\epsilon)^2\,\pi\rho_0(\mu)}-\frac{c(1-c)(\Delta\epsilon)^2\,\pi\rho_0(\mu)}{\Omega_B\,v_F\hbar}, \tag{2.32}$$

where the first term is Nordheim's rule. The second term, which comes from the nonvanishing vertex correction, represents a *deviation* from Nordheim's rule. While this deviation is strictly correct in the limit of small disorder, it is interesting to note the $\tilde{\sigma}(\omega=0,T=0)$ goes to 0 at

$$c=c_{\mathrm{crit}}=\tfrac{1}{2}(1\pm\sqrt{1-4\alpha}), \tag{2.33}$$

where $4\alpha<1$. This bound provides a limit of applicability of our approximations. We note that α is given by

$$\alpha=\left[\frac{\tilde{\rho}\Omega_B\,v_F\hbar}{\pi^2(\epsilon_A-\epsilon_B)^2\rho_0^2}\right]^{1/2}. \tag{2.34}$$

The lower root should be taken for $c_{\rm crit}$ as this root gives the proper dependence on the various parameters. To see this in a rough fashion for a simple cubic lattice, set

$$\tilde{\rho} \approx t^2 a^2 \rho_0 , \ \Omega_B = (2\pi/a)^3, \ \rho_0 \approx 1/(6t + |\epsilon_A - \epsilon_B|)$$

(a flat density of states). We then see that as t the hopping integral and v_F increase, $c_{\rm crit}$ increases. As $|\epsilon_A - \epsilon_B|$ and the lattice spacing (a) increase, $c_{\rm crit}$ decreases. This is in accordance with intuition.

ACKNOWLEDGMENTS

Work at City College was supported in part by the Army Reseach Office and the Department of Energy. Helpful conversations with T. Kaplan of Oak Ridge National Laboratories during the early part of the work described here is gratefully acknowledged.

[1]S. M. Chitanvis and R. Raghavan, Phys. Rev. B **28**, 5964 (1983).
[2]D. Langreth and E. Abrahams, Phys. Rev. B **24**, 2978 (1981).
[3]J. D. Bjorken and S. D. Drell, *Relativistic Quantum Field Theory II* (McGraw Hill, New York, 1965).
[4]R. L. Mills and P. Ratanavararaksa, Phys. Rev. B **18**, 5291 (1978).
[5]S. M. Chitanvis and P. L. Leath, J. Phys. C **16**, 1049 (1983).
[6]S. M. Chitanvis (unpublished).
[7]J. Langer and T. Neal, Phys. Rev. Lett. **16**, 984 (1966).
[8]E. Abrahams, P. W. Anderson, D. C. Licciardello, T. V. Ramakrishnan, Phys. Rev. Lett. **42**, 693 (1979).
[9]R. N. Bhatt and T. V. Ramakrishnan, Phys. Rev. B **28**, 6091 (1983).
[10]E. Abrahams and T. V. Ramakrishnan, J. Non-Cryst. Solids **35**, 15 (1980).
[11]B. Velický, Phys. Rev. **184**, 614 (1969).
[12]A. B. Chen and A. Sher, J. Vac. Sci. Technol. **21**, 138 (1982).